Proc. R. Soc. Lond. A **407**, 435–458 (1986)
Printed in Great Britain

Void growth in shear

BY N. A. FLECK[1] AND J. W. HUTCHINSON[2]

[1] *University Engineering Department, Trumpington Street, Cambridge CB2 1PZ, U.K.*

[2] *Division of Applied Sciences, Harvard University, Cambridge, Massachusetts* 02138, *U.S.A.*

(*Communicated by B. A. Bilby, F.R.S. – Received* 25 *February* 1986)

The growth of an isolated void is analysed for a void contained in a block of material undergoing simple shearing combined with superimposed hydrostatic tension. The evolution of the size, shape and orientation of two- and three-dimensional voids in an incompressible, linearly viscous solid is first discussed. The main problem addressed is the behaviour of a two-dimensional cylindrical void in an incompressible, nonlinearly viscous solid for which the strain rate varies as the stress to a power. The growth rate of the void and its shape evolution are strong functions of the degree of material nonlinearity. Relatively simple approximate formulas are obtained for the dilatation rate of a circular void as well as for the void potential. The constitutive relation of a block of material containing a dilute distribution of circular cylindrical voids is obtained directly using the isolated void potential. The paper concludes with a summary of available results for the dilatation rates of voids and cracks under combinations of shear and hydrostatic tension.

1. INTRODUCTION: VOID IN A LINEARLY VISCOUS MATERIAL

The present study is intended to provide insight into the void growth mechanism of ductile failure in solids under shearing deformations. The work builds on the pioneering work of McClintock *et al.* (1966) concerned with the behaviour of voids in shear bands. Aside from this early work, relatively little is known about void growth in metals under predominantly shearing conditions. Such knowledge is also needed for the further development of quantitatively accurate constitutive relations for porous metals.

This introduction will review some of the basic results of McClintock *et al.* (1966) for isolated 2D cylindrical voids in shearing fields and will compare them with some new results for 3D ellipsoidal voids, in both instances for incompressible linearly viscous materials. It will be seen that the 2D void in plane strain is a good model of the 3D void. The body of the paper then deals with various aspects of the behaviour of an isolated 2D cylindrical void of circular or elliptical cross section in a nonlinear power-law viscous solid. The geometry and notation used throughout the paper is displayed in figure 1. The field remote from the void is a state of simple shearing parallel to the x_1-direction with hydrostatic tension (or

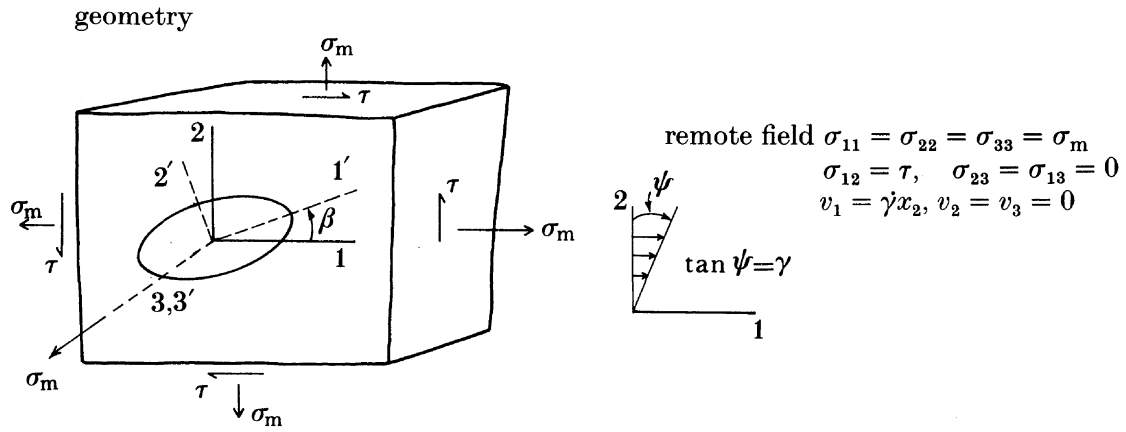

FIGURE 1. Conventions and remote stress and velocity fields.

pressure) superimposed on the incompressible material. The remote field is thus specified by the velocities

$$v_1^\infty = \dot{\gamma} x_2, \quad v_2^\infty = v_3^\infty = 0, \tag{1.1}$$

where $\dot{\gamma}$ is the remote shear strain rate; γ is the measure of shear used throughout, which will be referred to simply as the shear strain. The associated non-zero components of the remote strain rate, vorticity and stress are

$$\epsilon_{12}^\infty = \tfrac{1}{2}\dot{\gamma}, \quad \omega_{12}^\infty = \tfrac{1}{2}\dot{\gamma} \tag{1.2}$$

and

$$\sigma_{11}^\infty = \sigma_{22}^\infty = \sigma_{33}^\infty \equiv \sigma_m \quad \text{and} \quad \sigma_{12}^\infty \equiv \tau. \tag{1.3}$$

In all cases considered in this paper, the initial orientation and location of the void are such that it remains centred at the origin preserving symmetry with respect to the plane $x_3 = 0$. For 2D cylindrical voids the deformation is one of plane strain and thus independent of x_3.

All possible remote plane strain stress states are generated from all combinations of σ_m and τ. One important case is that of a void in a shear band which is at 45° to the axis of tension in a block of material undergoing plane strain tension σ. The void experiences a simple shearing history with $\sigma_m = \tau = \frac{1}{2}\sigma$, assuming the voids are relatively far apart. The ratio σ_m/τ will be used as the measure of stress triaxiality in this paper.

We begin by considering a void in an incompressible linearly viscous material whose strain rate is

$$\epsilon_{ij} = s_{ij}/(2\eta), \tag{1.4}$$

where $\boldsymbol{s}$ is the stress deviator. It is known from Eshelby's (1957) general solution that an ellipsoidal void will evolve through a sequence of ellipsoidal shapes. Throughout the paper, the major axis of the ellipsoidal void in the plane of x_1 and x_2 will be denoted by a and is aligned with x_1', while the minor axis in this plane is denoted by b and is aligned with x_2'. The axis of the ellipsoid in the direction of $x_3 = x_3'$ is c.

The solution for the evolution of a 2D cylindrical void was obtained by

McClintock *et al.* (1966) using Muskhelishvili methods. Here we note that their solution for the void surface can be represented compactly using the complex quantities R and m according to

$$x_1 + \mathrm{i}x_2 = R(\zeta + m/\zeta), \quad R \equiv |R|\,\mathrm{e}^{\mathrm{i}\alpha}, \quad m \equiv |m|\,\mathrm{e}^{\mathrm{i}\lambda}, \tag{1.5}$$

which maps the unit circle in the complex ζ-plane onto an ellipse centred in the plane of x_1 and x_2 with

$$a = |R|\,(1+|m|), \quad b = |R|\,(1-|m|), \quad \beta = \alpha + \tfrac{1}{2}\lambda. \tag{1.6}$$

The solution for the elliptical surface of a void, which is characterized by R_0 and m_0 when $\gamma = 0$ is

$$R = R_0\,\mathrm{e}^{[-\mathrm{i}+(\sigma_\mathrm{m}/\tau)]\frac{1}{2}\gamma}, \tag{1.7}$$

$$m = m_0\,\mathrm{e}^{-(\sigma_\mathrm{m}/\tau)\gamma} + \mathrm{i}\,\mathrm{e}^{-2\mathrm{i}\alpha_0}\,[\mathrm{i}+(\sigma_\mathrm{m}/\tau)]^{-1}\,(\mathrm{e}^{\mathrm{i}\gamma} - \mathrm{e}^{-(\sigma_\mathrm{m}/\tau)\gamma}). \tag{1.8}$$

For a void which is initially a circular cylinder of radius a_0 the above becomes

$$R = a_0\,\mathrm{e}^{[-\mathrm{i}+(\sigma_\mathrm{m}/\tau)]\frac{1}{2}\gamma}, \tag{1.9}$$

$$m = \mathrm{i}[\mathrm{i}+(\sigma_\mathrm{m}/\tau)]^{-1}\,(\mathrm{e}^{\mathrm{i}\gamma} - \mathrm{e}^{-(\sigma_\mathrm{m}/\tau)\gamma}). \tag{1.10}$$

The broken-line curves in figures 2, 3 and 4 show the evolution of a 2D cylindrical void which is initially circular and which is subject to constant ratios of σ_m/τ. The solid-line curves in these figures apply to an initially spherical void and will be discussed later. The ratio of void volume to initial volume when $\gamma = 0$ (i.e. the ratio of the respective cross sectional areas), V/V_0, is plotted as a function of shear strain γ in figure 2. When the mean stress σ_m is zero, the void closes at a shear strain of $\gamma = \cos^{-1}\frac{1}{2} = 1.05$, as can be seen most clearly in figure 4. If $\sigma_\mathrm{m}/\tau \leqslant 0.62$ the void closes and the limiting case for $\sigma_\mathrm{m}/\tau = 0.62$ is included in figure 2. The strain at closure for this case is $\gamma = 2.45$. For $\sigma_\mathrm{m}/\tau > 0.62$ the void remains open during the entire shearing history.

An interesting feature is brought out in figure 3, where the dilatation rate $\dot{V}/V$ of the void is normalized by the dilatation rate of a circular cylindrical void

$$\dot{V}/V = \sigma_\mathrm{m}/\eta, \tag{1.11}$$

at the same level of σ_m/τ. After a transient period when the dilatation rate drops below that of the circular cylindrical void, the dilatation rate asymptotes to the value for the circular cylindrical void, even though the asymptotic shape of the void is elliptical and not circular. Analogous behaviour is seen for the 3D void, which asymptotes to the dilatation rate of a spherical void, as will be discussed below. This same asymptotic behaviour was noted by Budiansky *et al.* (1982) for spheroidal voids under general axisymmetric remote stresses. These three instances lead us to make the following unproven conjecture. The dilatation rate of any 3D ellipsoidal (or 2D elliptical) void, which approaches a non-degenerate asymptotic shape in a given remote field will approach the dilatation rate of a spherical (or circular cylindrical) void in the same remote field.

The evolution of the orientation β of the major axis of the 2D cylindrical void and its aspect ratio b/a are shown in figure 4. When $\sigma_\mathrm{m}/\tau = 0$, the curve is

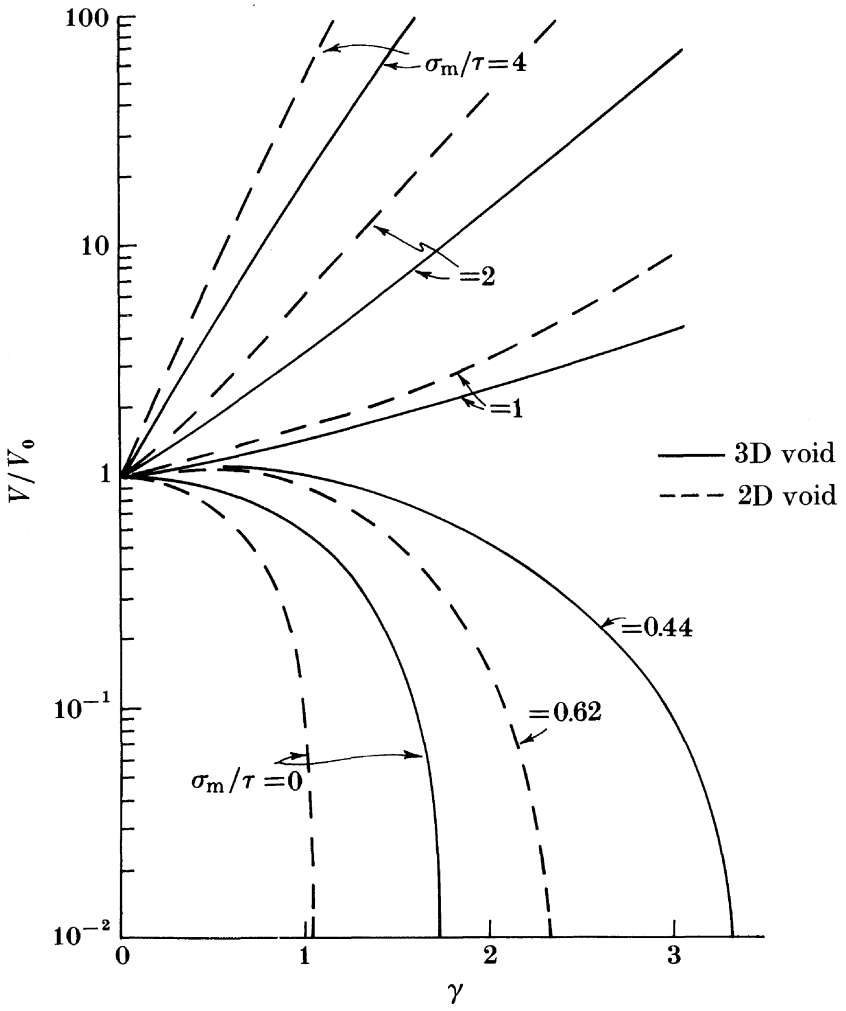

FIGURE 2. Ratio of volume of void at shear strain γ to initial volume at different triaxiality ratios σ_m/τ. Starting shape for 3D void is a sphere and for 2D void is a circular cylinder ($n = 1$).

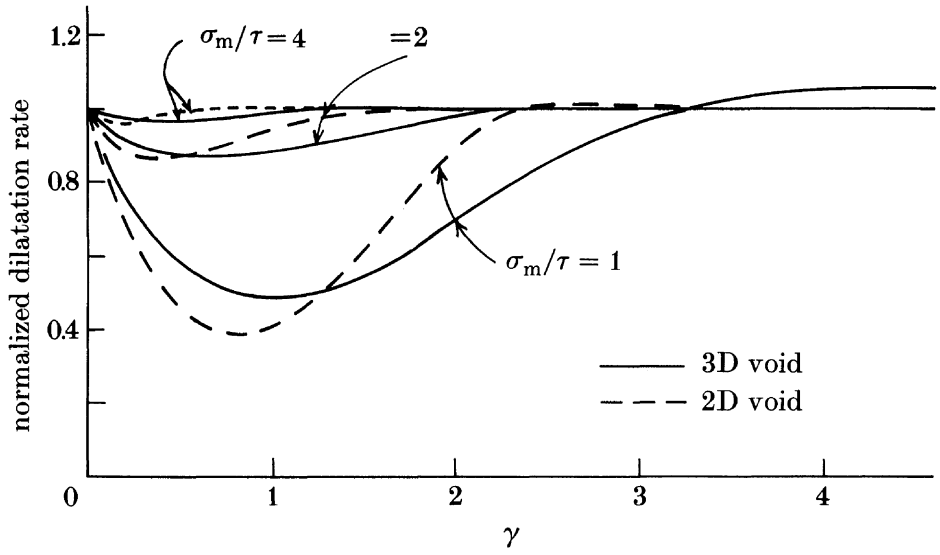

FIGURE 3. Evolving ratio of dilatation rate to corresponding dilatation rate of sphere (for 3D void) or of circular cylinder (for 2D void). Equation (1.11) is used for normalizing the 2D case and (1.17) for the 3D case. Starting shape is a sphere for the 3D void and a circular cylinder for the 2D void ($n = 1$).

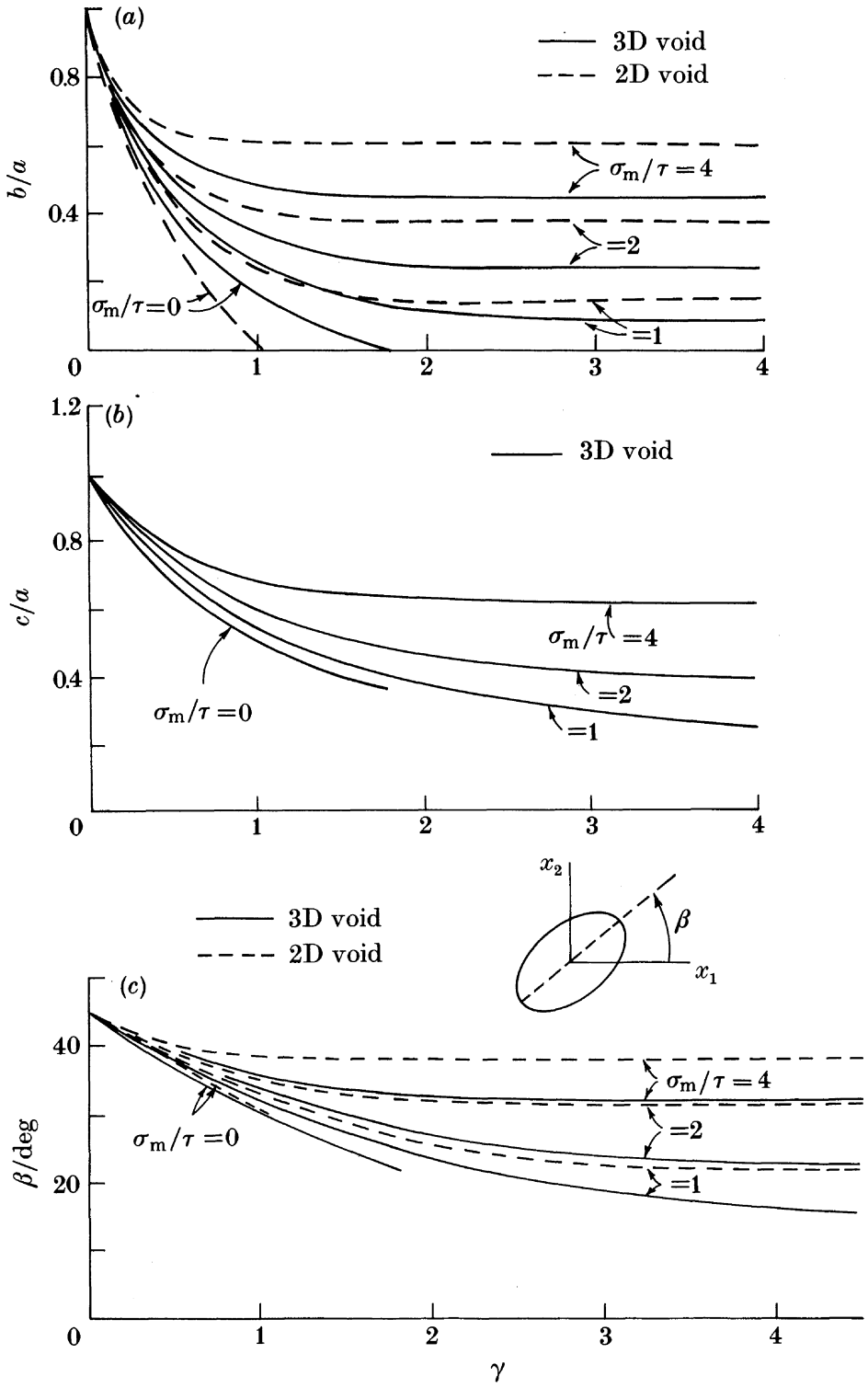

FIGURE 4. Evolution of the aspect ratios and orientation of 2D and 3D voids. Corresponding evolution of the volume is given in figure 2 ($n = 1$).

terminated at $\beta \approx 30°$ and $\gamma = 1.05$ when the void closes. For $\sigma_m/\tau > 0.62$ the void approaches an orientation inclined to the x_1 axis and a finite asymptotic aspect ratio b/a.

An isolated void starting with a spherical shape when $\gamma = 0$ evolves through a sequence of ellipsoidal shapes when subject to the remote field (1.1)–(1.3). The solution can be obtained by specializing Eshelby's (1957) general solution for

ellipsoidal inclusions. Related studies for cavities containing a second incompressible linearly viscous material have been carried out by Bilby *et al.* (1975), Howard & Brierley (1976) and Bilby & Kolbuszewski (1977). The last authors also discuss the equations governing the evolution of a vacuous ellipsoidal void, and the formulation outlined below is essentially identical to theirs.

Let $\boldsymbol{L}$ be the uniform viscous moduli of the material outside the void such that $\sigma_{ij} = L_{ijkl}\,\epsilon_{kl}$. Under the remote stress $\boldsymbol{\sigma}^\infty$ and the remote vorticity $\boldsymbol{\omega}^\infty$, the surface of the void deforms through a sequence of ellipsoidal shapes, as already emphasized, and one can regard the 'ether' in the void as undergoing a uniform strain rate $\boldsymbol{\varepsilon}^{\mathrm{c}}$ and a uniform vorticity $\boldsymbol{\omega}^{\mathrm{c}}$. If the ellipsoidal surface of the void is specified by

$$G_{ij}\,x_i\,x_j = 1, \tag{1.12}$$

then (Goddard & Miller 1967)

$$\dot{G}_{ij} = -G_{ip}(\epsilon^{\mathrm{c}}_{pj}+\omega^{\mathrm{c}}_{pj}) - G_{jp}(\epsilon^{\mathrm{c}}_{pi}+\omega^{\mathrm{c}}_{pi}). \tag{1.13}$$

For the special remote conditions (1.1)–(1.3) of interest here, the void retains its symmetry with respect to the x_3 direction, $\epsilon^{\mathrm{c}}_{13} = \epsilon^{\mathrm{c}}_{23} = \omega^{\mathrm{c}}_{13} = \omega^{\mathrm{c}}_{23} = 0$, and one can use (1.13) to obtain

$$\dot{\beta} = (a^2+b^2)\,(a^2-b^2)^{-1}\,\epsilon^{\mathrm{c}}_{1'2'} - \omega^{\mathrm{c}}_{1'2'}, \tag{1.14}$$

where the primes denote components in non-rotating axes, x'_1, which are momentarily coincident with the principal axes of the ellipsoid, as indicated in figure 1.

The strain rate and vorticity in the void are determined from

$$(L_{ijkl} - L_{ijmn}\,S_{mnkl})\,\epsilon^{\mathrm{c}}_{kl} = \sigma^\infty_{ij} \tag{1.15}$$

and

$$\omega^{\mathrm{c}}_{ij} - \omega^\infty_{ij} = \Pi_{ijkl}\,\epsilon^{\mathrm{c}}_{kl}, \tag{1.16}$$

where $\boldsymbol{S}$ and $\boldsymbol{\Pi}$ are the special tensors introduced by Eshelby (1957) to solve the ellipsoidal transformation problem. Equations (1.15) and (1.16) will not be specialized further here. Our solution procedure entailed writing these equations in the x'_i-axes and then using Eshelby's expressions for the components of $\boldsymbol{S}$ and $\boldsymbol{\Pi}$. The above equations are supplemented by $\dot{a} = a\epsilon^{\mathrm{c}}_{1'1'}$, $\dot{b} = b\epsilon^{\mathrm{c}}_{2'2'}$ and $\dot{c} = c\epsilon^{\mathrm{c}}_{3'3'}$.

The behaviour of the void as it evolves from a starting spherical shape at $\gamma = 0$ is shown alongside the 2D results in figures 2, 3 and 4. When $\sigma_{\mathrm{m}} = 0$, the void closes (i.e. $b \to 0$ with $c/a \to 0.37$) at a shear strain $\gamma = 1.76$. For $\sigma_{\mathrm{m}}/\tau > 0.44$, the void does not close. The transition case with $\sigma_{\mathrm{m}}/\tau = 0.44$ is included in figure 2; closure occurs at $\gamma = 3.4$. As already mentioned, the dilatation rate of the 3D void asymptotes to the rate for the spherical void,

$$\dot{V}/V = \tfrac{3}{4}\sigma_{\mathrm{m}}/\eta, \tag{1.17}$$

when $\sigma_{\mathrm{m}}/\tau > 0.44$, as can be seen in figure 3.

At corresponding levels of σ_{m}/τ the 3D void evolves to its asymptotic shape and orientation somewhat more slowly than its 2D counterpart. Its dilatation rate, $\dot{V}/V$, is also slightly lower. For the most part, however, the 2D cylindrical void appears to be a good qualitative model of the 3D void.

2. Deformation rate of cylindrical voids of circular and elliptical cross section in a nonlinearly viscous matrix

In this section a method is detailed for the numerical solution of the 2D problem of a cylindrical void of elliptical cross section in an infinite power-law viscous matrix subject to the remote field (1.1)–(1.3). The matrix material is isotropic and incompressible with a uniaxial strain rate in simple tension given by

$$\epsilon = \epsilon_0(\sigma/\sigma_0)^n, \tag{2.1}$$

where ϵ_0 and σ_0 are a reference strain rate and stress. Under multiaxial stress states σ_{ij}, (2.1) generalizes to

$$\epsilon_{ij} = \sigma_e^{n-1} s_{ij}/(2\eta), \tag{2.2}$$

where $\boldsymbol{\varepsilon}$ is the strain rate, $\boldsymbol{s}$ is the stress deviator, $\sigma_e = (3s_{ij}\,s_{ij}/2)^{\frac{1}{2}}$ is the effective stress, and η is a viscosity-like parameter defined by

$$\eta = \sigma_0^n/(3\epsilon_0). \tag{2.3}$$

An effective strain rate $\epsilon_e = (2\epsilon_{ij}\,\epsilon_{ij}/3)^{\frac{1}{2}}$ is also defined such that the relation between ϵ_e and σ_e is the same as the tensile law, i.e.,

$$\epsilon_e = \epsilon_0(\sigma_e/\sigma_0)^n = \sigma_e^n/(3\eta). \tag{2.4}$$

For $n = 1$ this relation reduces to the linearly viscous law considered in §1. At the other limit, $n \to \infty$, it becomes a rigid or perfectly plastic material with the yield condition $\sigma_e = \sigma_0$.

2.1. *Radially symmetric solution*

For reference, we give the exact solution, which can be obtained analytically, for a circular cylindrical void of radius a in a matrix with finite outer radius a_0 when a normal traction T acts on the outer cylinder surface. The dilatation rate of the void is found to be

$$\dot{V}/V = 2v_r(a)/a = (1/(\eta\sqrt{3}))\,\mathrm{sgn}\,(T)\,(|T|\sqrt{3}/n)^n(1-\rho^{1/n})^{-n}, \tag{2.5}$$

where the area fraction $\rho = (a/a_0)^2$ can be thought of as the void volume fraction, and $\mathrm{sgn}\,(T) = T/|T|$. In the limit $a_0 \to \infty$, $T \to \sigma_m$ and (2.5) reduces to

$$\dot{V}/V = (1/(\eta\sqrt{3}))\,\mathrm{sgn}\,(\sigma_m)\,(|\sigma_m|\sqrt{3}/n)^n. \tag{2.6}$$

As in the spherically symmetric void problem discussed by Budiansky *et al.* (1982), the lowest order influence of the void volume fraction on the dilatation rate is proportional to $\rho^{1/n}$. Thus, interaction between voids can be expected to occur at exceedingly low values of ρ when n is large and when the overall stress state is one of hydrostatic tension or compression.

2.2. *Numerical technique*

We first describe the procedure for computing the velocity field and then explain the method for determining the deformation rate of the void from the velocity field.

A minimum principle for velocities was employed to find approximate Rayleigh–Ritz solutions. The principle is from Hill (1956) and was modified by Budiansky *et al.* (1982) to be applicable to infinite regions. With $\boldsymbol{v}^\infty$, $\boldsymbol{\varepsilon}^\infty$, $\boldsymbol{\sigma}^\infty$ denoting quantities associated with the remote field, as in (1.1)–(1.3), the complete field is written as

$$v_{i,j} = v^\infty_{i,j} + \tilde{v}_{i,j}, \quad \epsilon_{ij} = \epsilon^\infty_{ij} + \tilde{\epsilon}_{ij}, \quad \sigma_{ij} = \sigma^\infty_{ij} + \tilde{\sigma}_{ij}, \tag{2.7}$$

where the additional fields, which are denoted by a superscript tilde, decay to zero at infinity. The strain rates and velocities are connected by

$$\epsilon^\infty_{ij} = (v^\infty_{i,j} + v^\infty_{j,i})/2 \quad \text{and} \quad \tilde{\epsilon}_{ij} = (\tilde{v}_{i,j} + \tilde{v}_{j,i})/2, \tag{2.8}$$

while $\boldsymbol{\sigma}$ and $\boldsymbol{\varepsilon}$ are related by (2.2).

Subject to conditions on the rate of decay of the additional velocity fields admitted for consideration, the exact field minimizes

$$P(\tilde{\boldsymbol{v}}) = \int_V \{w(\boldsymbol{\varepsilon}) - w(\boldsymbol{\varepsilon}^\infty) - \sigma^\infty_{ij}\,\tilde{\epsilon}_{ij}\}\,\mathrm{d}V - \int_S \sigma^\infty_{ij}\,n_j\,\tilde{v}_i\,\mathrm{d}S, \tag{2.9}$$

where V is the infinite region surrounding the void, S is the void surface, and $\boldsymbol{n}$ is the unit normal pointing into V. The potential $w(\boldsymbol{\varepsilon})$ is defined by

$$w(\boldsymbol{\varepsilon}) = \int_0^{\boldsymbol{\varepsilon}} \sigma_{ij}\,\mathrm{d}\epsilon_{ij} = \sigma_0\,\epsilon_0 \left(\frac{n}{n+1}\right)\left(\frac{\epsilon_e}{\epsilon_0}\right)^{(n+1)/n} \tag{2.10}$$

so that $s_{ij} = \partial w/\partial \epsilon_{ij}$. In 2D applications the minimum principle is restricted to problems for which the additional strain rates $\tilde{\boldsymbol{\varepsilon}}$ decay faster than r^{-1} where $r^2 = x_i\,x_i$, and the admissible class of trial functions must meet this restriction. As long as n is finite, the solution for the additional strain rates in the present problems decays like r^{-2}. This is not necessarily true for the rigid or perfectly plastic solid ($n \to \infty$), and we will not attempt solutions for this limit. The governing equations are elliptic when n is finite but may become hyperbolic in the limit $n \to \infty$.

A mapping technique was used in conjunction with the minimum principle to deal with cylindrical voids of elliptic cross section. Let $z = x_1 + \mathrm{i}x_2 = r\mathrm{e}^{\mathrm{i}\theta}$ be a complex variable defined in the physical plane and $\zeta = \xi_1 + \mathrm{i}\xi_2 = \mu\mathrm{e}^{\mathrm{i}\phi}$ be the variable in the mapped plane. The region exterior to the elliptical boundary of the void is mapped onto the interior of the unit circle in the ζ-plane by (1.5), where now R is taken to be real. Thus, as indicated in figure 5,

$$a = R(1+|m|), \quad b = R(1-|m|), \quad \beta = \tfrac{1}{2}\lambda, \tag{2.11}$$

where a is the length of the semimajor axis of the ellipse, b the length of the semiminor axis, and β is the orientation of the semimajor axis.

Incompressibility of the additional velocity fields was satisfied with the aid of a stream function $\chi(x_1, x_2)$ such that

$$\tilde{v}_1 = \chi_{,2}, \quad \tilde{v}_2 = -\chi_{,1}. \tag{2.12}$$

The stream function was regarded as a function of the polar coordinates (μ, ϕ) in

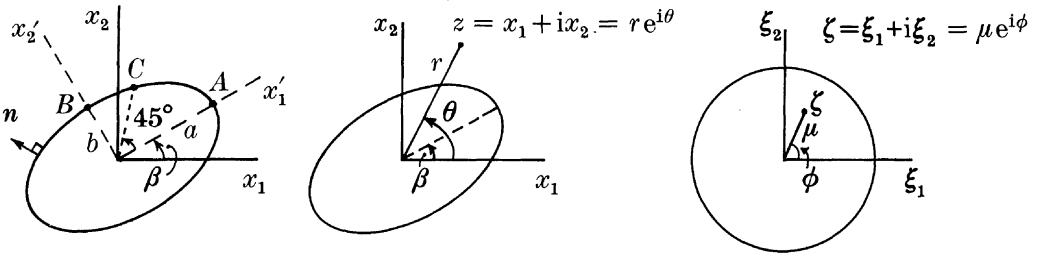

FIGURE 5. Geometry and mapping from physical plane to mapped plane.

the mapped plane. A truncated complete representation was employed according to

$$\chi = A\theta + \sum_{j=1}^{N} \sum_{k=1}^{M} \{A_{jk}\mu^{k-1} \sin 2j\phi + B_{jk}\mu^{k-1} \cos 2j\phi\}, \tag{2.13}$$

where the amplitudes A, A_{jk} and B_{jk} are free parameters chosen to minimize P. The lead term in (2.13), $A\theta$, gives rise to the radially symmetric contribution

$$\tilde{v}_r = Ar^{-1}, \; \tilde{v}_\theta = 0, \quad \tilde{\epsilon}_r = -\tilde{\epsilon}_\theta = -Ar^{-2}, \quad \tilde{\epsilon}_{r\theta} = 0. \tag{2.14}$$

This term, which is solely responsible for the dilatation rate, was retained in this simple form, although a multi-valued function of ϕ could have been used. The ϕ-dependence of the trigonometric terms in (2.13) is consistent with the periodicity of the solution in the physical plane.

The contributions to the velocity and strain rate fields from the terms other than $A\theta$ in (2.13) were computed using the change of variables specified by the mapping function, $z = \omega(\zeta)$, as detailed in the Appendix. In this way, additional velocities and strain rates can be computed at any point z corresponding to ζ in the mapped plane, given values prescribed to the free amplitudes. For a given void shape specified by $z = \omega(\zeta)$, the minimization of P with respect to the amplitude factors is conducted by a Newton–Raphson method. With the set of $K = 1 + 2MN$ free amplitude factors denoted by $\{A_p\}$, the condition for the minimum is

$$\partial P/\partial A_p = 0, \quad p = 1, K. \tag{2.15}$$

Given an estimate of the amplitudes as $\{A_p\}$, the improved estimate, $\{A_p + \Delta A_p\}$ is obtained from

$$\sum_{p=1}^{K} \frac{\partial^2 P}{\partial A_q \partial A_p} \Delta A_p = -\frac{\partial P}{\partial A_q}, \quad q = 1, K. \tag{2.16}$$

Explicit expressions for the partial derivatives which are evaluated at $\{A_p\}$, are

$$\frac{\partial P}{\partial A_p} = \int_V (\sigma_{ij} - \sigma_{ij}^\infty)\, \tilde{\epsilon}_{ij}^{(p)}\, \mathrm{d}V - \int_S \sigma_{ij}^\infty n_j \tilde{v}_i^{(p)}\, \mathrm{d}S \tag{2.17}$$

and

$$\frac{\partial^2 P}{\partial A_q \partial A_p} = \int_V 2\eta (3\eta \epsilon_e)^{-(n-1)/n} \left[\tilde{\epsilon}_{mn}^{(p)} \tilde{\epsilon}_{mn}^{(q)} - \frac{2(n-1)}{3n} \epsilon_e^{-2} \epsilon_{ij} \tilde{\epsilon}_{ij}^{(p)} \epsilon_{kl} \tilde{\epsilon}_{kl}^{(q)} \right] \mathrm{d}V, \tag{2.18}$$

where, in obvious notation,

$$\tilde{v}_i = \sum_{p=1}^{K} A_p \tilde{v}_i^{(p)} \quad \text{and} \quad \tilde{\epsilon}_{ij} = \sum_{p=1}^{K} A_p \tilde{\epsilon}_{ij}^{(p)}. \tag{2.19}$$

The integrations in (2.9), (2.17) and (2.18) were carried out numerically by using integration formulas with μ and ϕ as integration variables, as discussed in the Appendix. The numerical minimization procedure gave the deformation rate of a circular cylindrical void in a linear viscous material ($n = 1$) to an accuracy of six significant figures since the representation for χ contains the exact solution for this case ($A = \sigma_m^\infty a^2/(2\eta)$, $B_{11} = -2B_{13} = -\sigma_{12}^\infty a^2/(2\eta)$) and the integration formulas are also exact to within round-off error for the particular integrands. For the nonlinear material ($n > 1$), numerical experimentation with different N and M showed that the dilatation rate and the rate of change of the aspect ratio, $(a/b)^{\cdot}$, were accurate to better than 2%, while the rotation rate of the void, $\dot{\beta}$, was accurate to better than 5%, when $M = 4$ and $N = 3$, as long as the aspect ratio of the void did not exceed 2. A prohibitively large number of amplitude terms would be required to achieve accurate results for voids with greater aspect ratios.

Calculations were lengthy and a judicious starting choice was required for the amplitudes. A form of parameter tracking was employed whereby the starting values of the amplitudes were taken from the converged solution at a slightly lower n. Convergence problems became severe when n was greater than 5, reflecting the intensification of velocity gradients at high n.

The void in the linear material evolves through a sequence of elliptical shapes. This is not strictly true for the void in the nonlinear material, but examination of the velocity component normal to circular and elliptical voids indicated that the incremental shape change was closely approximated by a deforming ellipse. This observation facilitated the computation and presentation of the rates of change of the parameters characterizing the size, shape and orientation of the void.

The velocity component normal to the surface of a void deforming through a sequence of elliptical shapes is given by

$$v_n = \dot{\beta}(x_1' n_2' - x_2' n_1') + (\dot{a}/a) x_1' n_1' + (\dot{b}/b) x_2' n_2', \tag{2.20}$$

where $\dot{\beta}$ is the rotation rate of the major axis of the ellipse, x_i' are axes aligned with its principal axes, and n_i' are the components of the unit normal to the surface in these axes, as shown in figure 5. The quantities $\dot{a}/a$, $\dot{b}/b$ and $\dot{\beta}$ were determined from the three equations obtained from (2.20) by evaluating v_n from the numerical solution at the points A, B and C (see figure 5) on the ellipse. The normalized dilatation rate can be computed either directly from the contribution $A\theta$ to χ giving

$$\dot{V}/(\dot{\gamma} V) = 2A/(\dot{\gamma} ab), \tag{2.21}$$

or by using the values of $\dot{a}/a$ and $\dot{b}/b$ and the elliptical approximation, which give

$$\dot{V}/(\dot{\gamma} V) = (\dot{a}/a + \dot{b}/b)/\dot{\gamma}. \tag{2.22}$$

These two formulas always agreed to within a few percent, indicating that the

deformation rate of the void shape is well approximated by a deforming ellipse. The normalized rate of change of the aspect ratio was computed from

$$(a/b)^{\cdot}/\dot{\gamma} = (a/b)\,(\dot{a}/a - \dot{b}/b)/\dot{\gamma}. \tag{2.23}$$

2.3. *Numerical results*

Results characterizing the initial deformation rate of isolated cylindrical voids of circular and elliptical cross section are now presented for various n-values as a function σ_m/τ. We will regard τ and σ_m as being positive, but solutions for negative τ and/or σ_m can be deduced immediately from symmetry and the fact that changing the sign of $\boldsymbol{\sigma}^\infty$ simply changes the sign of the velocity. From (1.2) and (2.2) it is noted that the remote shear and vorticity rates are given by

$$\epsilon_{12}^\infty = \omega_{12}^\infty = \tfrac{1}{2}\dot{\gamma} = (|\tau|\sqrt{3})^{n-1}\tau/(2\eta). \tag{2.24}$$

The normalized dilatation rate of an elliptical void with aspect ratio 2 is compared with that of a circular void in figure 6. The dilatation rate necessarily

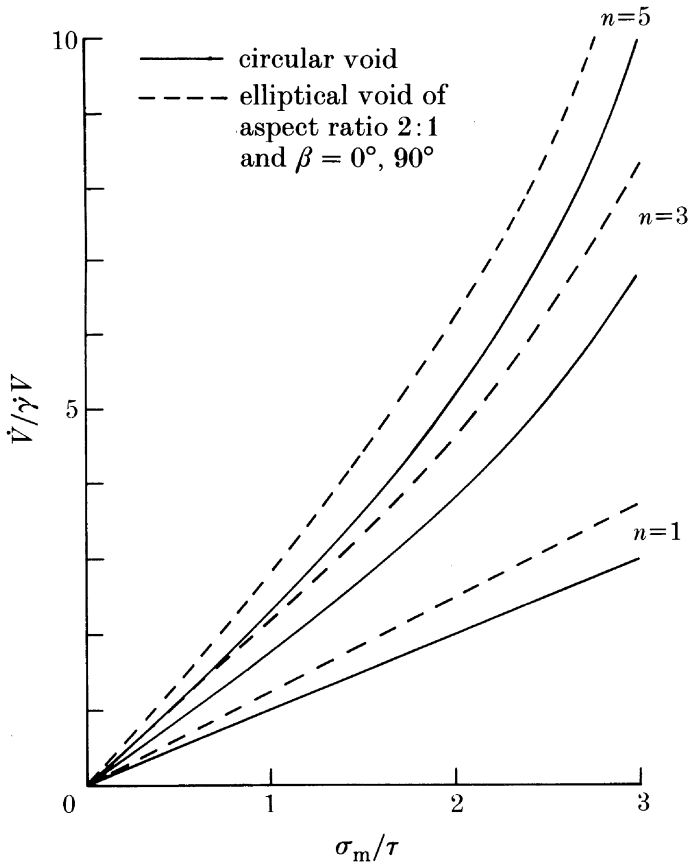

FIGURE 6. Normalized dilatation rate as a function of stress triaxiality for voids with circular and elliptical cross sections for several n-values.

vanishes when $\sigma_m = 0$. By symmetry, the result for the elliptical void apply equally well for the orientation $\beta = 0$ or $\beta = 90°$. While the normalized dilatation rate for the elliptical void is slightly larger (typically by about 20 % for each n-value shown), the dependence on the aspect ratio is not exceptionally strong. A stronger dependence on n and stress triaxiality σ_m/τ is seen.

The initial rate of change of the aspect ratio of the circular cylindrical void is shown in figure 7*a*. The point on the circular void surface where the normal velocity is a maximum locates the orientation β of the major axis of the evolving pseudo-ellipse, and this orientation is displayed in figure 7*b*. For $n = 1$, the circular void evolves into an ellipse with initial orientation of its major axis at $\beta = 45°$ to the x_1-axis for all levels of triaxiality. Similar behaviour is seen for the void in the nonlinear material ($n = 3$ or 5) when σ_m/τ is small. However, at higher triaxiality the behaviour changes dramatically. Above a certain triaxiality level depending on n, the evolving pseudo-ellipse is orientated with its major axis at $\beta \approx -45°$. We re-emphasize that a is always identified with the length of the major axis.Thus, the abrupt turn-up in figure 7*a* in the curve of $(a/b)^{\cdot}$ against σ_m/τ reflects the transition in orientation of the major axis. In figure 7*b*, the portions of the curves in this transition are broken as an indication that they have been drawn based on only relatively few points.

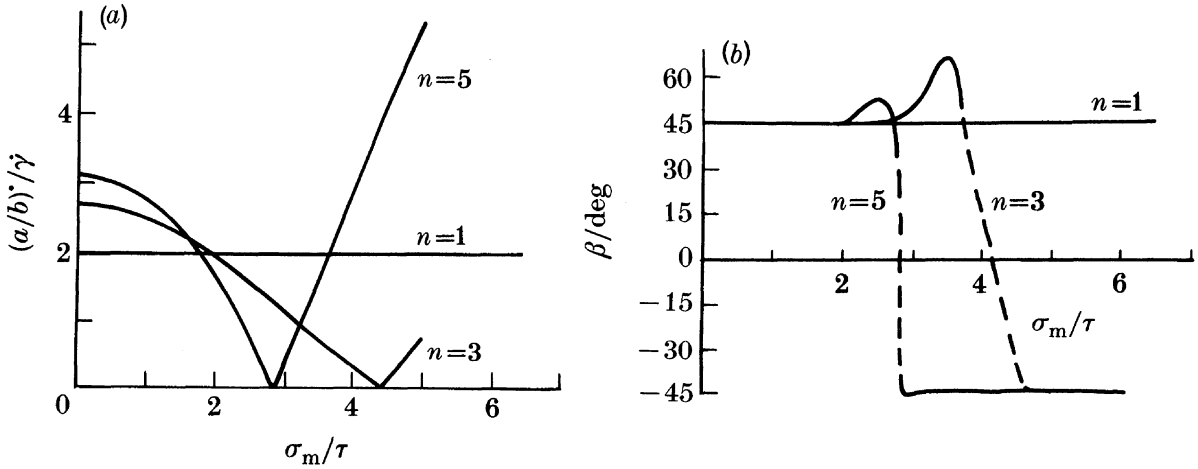

FIGURE 7. (*a*) Initial rate of change of aspect ratio and (*b*) initial orientation β of major axis for a void with a starting circular cross section as a function of stress triaxiality.

The results for $n = 1$ are in accord with one's physical intuition that the circular void should evolve into an ellipse with major axis aligned in the direction of maximum principal straining. Surprisingly, for the nonlinear material the void evolves instead into a pseudo-ellipse with major axis transverse to the direction of maximum principal straining when the stress triaxiality is sufficiently large. Budiansky *et al.* (1982) and Budiansky & Hutchinson (1980) have observed similarly that a spherical void in the nonlinear material under remote axisymmetric loading will deform into an oblate spheroid when the ratio of the remote mean to effective stresses is sufficiently large. The void grows more rapidly in directions perpendicular to the straining direction than along it. The explanation appears to be common to both the cylindrical void and the 3D void. Here attention will be restricted to the cylindrical void.

The anomalous behaviour in the nonlinear material under high triaxiality is a consequence of the nonlinear coupling between the remote shear field and the radially symmetric field. When σ_m/τ is large and $n > 1$, the radially symmetric

field dominates the deformation response of the void, and the strain rates and velocities in the vicinity of the void are given roughly by

$$\dot{\epsilon}_\theta = (\tfrac{1}{2}\sqrt{3})\,\dot{\epsilon}_e = -\dot{\epsilon}_r, \quad \dot{\epsilon}_{r\theta} = 0, \tag{2.25}$$

$$v_r = r\dot{\epsilon}_\theta = (\tfrac{1}{2}\sqrt{3})r\dot{\epsilon}_e, \quad v_\theta = 0. \tag{2.26}$$

The main pertubing effect of the remote strain rate $\dot{\gamma}$ is to alter the variation of $\dot{\epsilon}_e$ near the void with less effect on the relative proportions of the components in (2.25) and (2.26). For positive $\dot{\gamma}$, $\dot{\epsilon}_e$ is largest at $\theta = -45°$ and $135°$, and smallest at $\theta = 45°$ and $-135°$, as one would expect. With (2.26) still approximately in effect, this implies that the void grows fastest in the directions $\theta = -45°$ and $135°$ transverse to the direction of maximum remote principal straining.

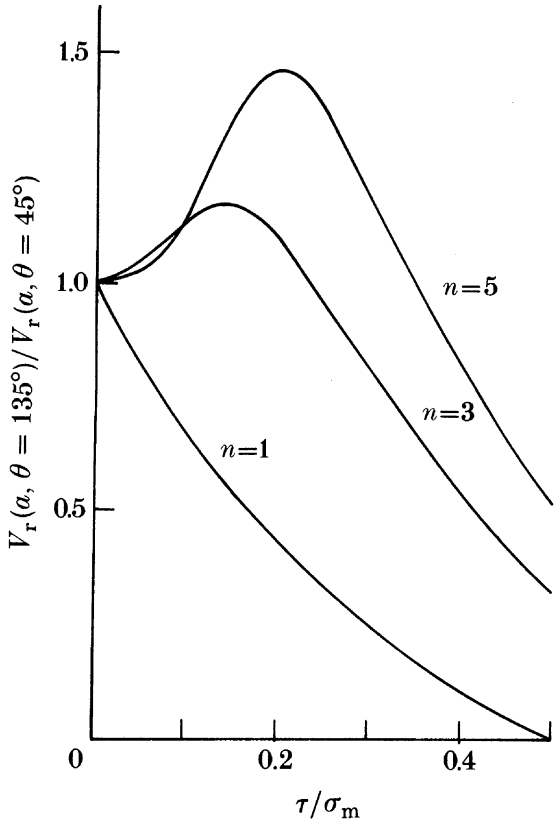

FIGURE 8. Ratio of velocity normal to surface of circular void at $\theta = 135°$ to that at $\theta = 45°$, as a function of τ/σ_m. The void in the nonlinear material grows more rapidly in the direction perpendicular to the maximum principal strain rate than along it at sufficiently large triaxiality (i.e. sufficiently small τ/σ_m).

The tendency just discussed can be seen directly in figure 8 where for a circular void the ratio of v_r ($r = a$, $\theta = 135°$) to v_r ($r = a$, $\theta = 45°$) is shown as a function of τ/σ_m for $n = 1$, 3 and 5. For $n = 1$, this ratio diminished monotonically from unity as τ/σ_m increases, indicating that the void elongates in the direction of maximum principal straining. For $n > 1$, there is a range of τ/σ_m where the void clearly grows faster in the transverse direction.

We now consider the rotation rate $\dot{\beta}$ of the major axis of a void which at the current instant has an elliptical cross section with aspect ratio 2 and whose

orientation β with respect to the x_1-axis can take on any value between $-90°$ and $90°$. Results for a relatively low triaxiality, $\sigma_m/\tau = 1$, are shown in figure 9 and for a high triaxiality, $\sigma_m/\tau = 5$, in figure 10. For the low triaxiality case in figure 9, there are two orientations, $\beta \approx \pm 35°$, for which the void is momentarily not rotating. The orientation $\beta \approx 35°$ is stable for all n since a void slightly rotated from this orientation will rotate back towards it. Conversely, the orientation $\beta \approx -35°$ is unstable. At high triaxiality in figure 10, it is seen that for $n = 1$ the orientation $\beta \approx 30°$ is again the stable one. However, for $n = 3$ and $n = 5$ the

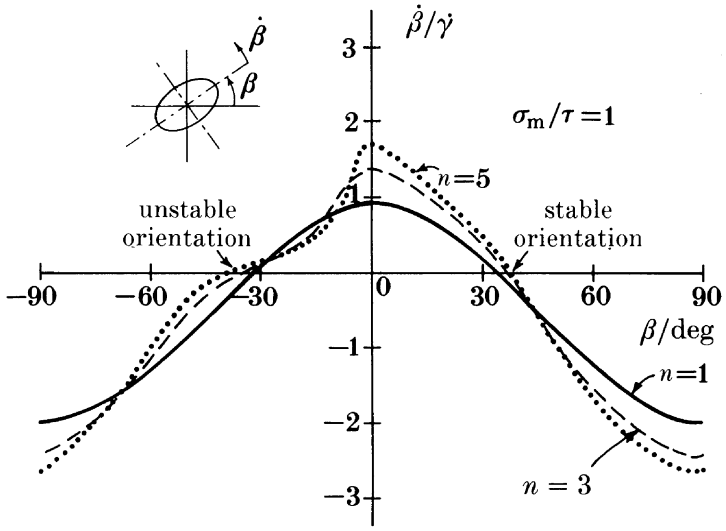

FIGURE 9. Rate of rotation $\dot{\beta}$ of the maximum principal axes of an elliptical void with a current aspect ratio of 2 as a function of the void orientation β for $\sigma_m/\tau = 1$.

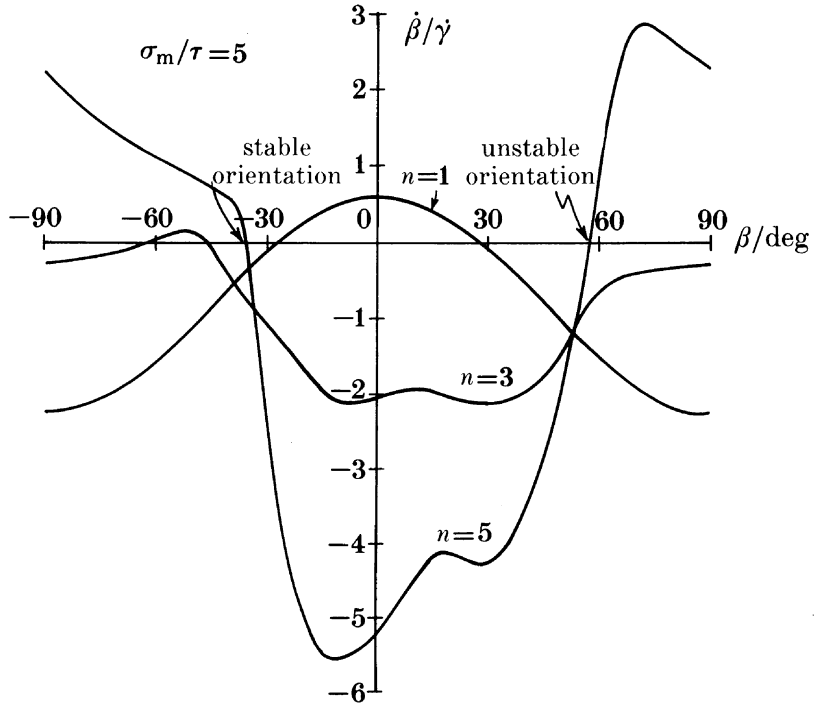

FIGURE 10. Rate of rotation $\dot{\beta}$ of the maximum principal axis of an elliptical void with a current aspect ratio of 2 as a function of the void orientation β for $\sigma_m/\tau = 5$.

stable orientations are at angles of about $-45°$ and $-35°$, respectively. This behaviour is consistent with the initial deformation rate of the circular cylindrical void.

3. Evolution of an initially circular cylindrical void

To illustrate the evolution of the void shape and orientation, an initially circular cylindrical void is considered subject to the triaxiality ratio $\sigma_m/\tau = 4$. From the results of figure 7*b* giving the initial deformation rate, we can expect a void in the most nonlinear material ($n = 5$) to evolve to an orientation with its major axis transverse to the principal straining direction. The calculations were made with the numerical scheme outlined in the previous section. The void dimensions, a and b, and orientation, β, were updated after small increments in time (or remote strain) such that in each increment the largest in magnitude of $\Delta a/a$ and $\Delta b/b$ was less than 0.1, while $\Delta\beta$ never exceeded 5°. The results of the calculation are shown in figure 11, and are now discussed.

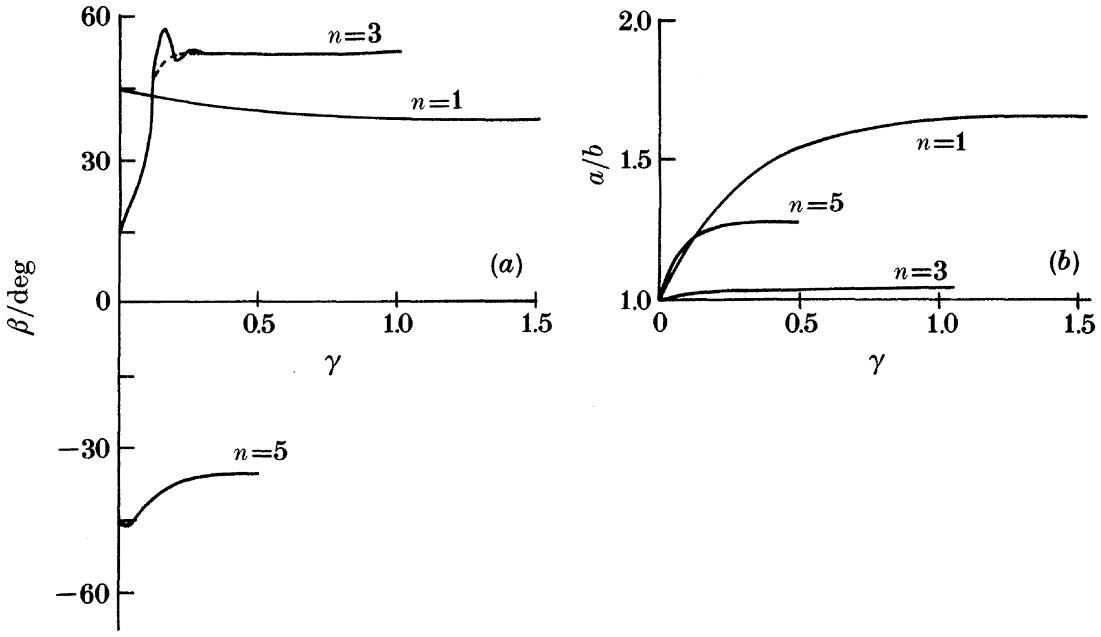

Figure 11. Evolution of orientation and aspect ratio of an initially circular void in linear and nonlinear materials for $\sigma_m/\tau = 4$.

For $n = 1$ the circular void evolves into an ellipse of aspect ratio $a/b = 1.64$ and inclination $\beta = 38°$ after a shear strain γ of approximately unity. For $n = 3$, the void remains almost circular and asymptotes to an aspect ratio $a/b = 1.03$ and an inclination $\beta = 52°$. For $n = 5$, the void evolves to an aspect ratio $a/b = 1.27$ with an inclination $\beta = -36°$, as expected, after a shear strain of about 0.3. For all n considered, the dilatation rate of the void remained to within 1 % of the dilatation rate for a circular void at the same triaxiality level over the whole history. The small oscillation in β for the case $n = 3$ as the void evolves to its asymptotic shape is thought to be spurious. It is a consequence of the finite step size in the numerical

procedure and the fact that β is difficult to identify when the shape is almost circular.

At lower triaxiality the asymptotic void shapes will have larger aspect ratios. For $n = 1$, the results of McClintock *et al.* (1966) show that the asymptotic aspect ratios are larger than 2 when σ_m/τ is less than 3. Numerical experimentation indicated that the same will be true for the nonlinearly viscous materials. Since the accuracy of the numerical technique is severely diminished when $a/b > 2$, no attempt was made to track the evolution in the nonlinear material for $\sigma_m/\tau < 3$.

It is concluded that a circular void will evolve into a pseudo-ellipse with major axis aligned approximately transverse to the direction of maximum principal straining when σ_m/τ is sufficiently large and when the material is nonlinear. Otherwise, it evolves into an ellipse or pseudo-ellipse with major axis approximately aligned with the direction of maximum principal straining. It is seen that the asymptotic void shape tends to be achieved after considerably less strain in the nonlinear material than in the linear material.

4. Approximations to the dilatation rate of a circular cylindrical void

4.1. *High triaxiality approximation*

When the triaxiality is large there is a strong coupling between the radially symmetric field and the remote shear field. A good approximation to the dilatation rate of a circular cylindrical void may be achieved by neglecting all but the radially symmetric term $A\theta$ in expression (2.13) for the stream function χ for the additional velocity field. The functional P in (2.9) then reduces to

$$P = 2\int_0^{\pi} \mathrm{d}\theta \int_a^{\infty} \left[\frac{n}{n+1} (3\eta)^{1/n} (\tfrac{4}{3})^{(n+1)/2n} \left\{ \left(\tfrac{1}{4}\dot\gamma^2 - \frac{\dot\gamma A \sin 2\theta}{r^2} + \frac{A^2}{r^4} \right)^{(n+1)/2n} - (\tfrac{1}{2}\dot\gamma)^{(n+1)/n} \right\} + 2\tau \frac{A}{r^2} \sin 2\theta \right] r \, \mathrm{d}r - 2\pi\sigma_m A. \quad (4.1)$$

Minimization of P with respect to the free amplitude A and use of the identity $\dot V/(\dot\gamma V) = 2A/(\dot\gamma a^2)$ leads to an expression relating the dilatation rate to σ_m/τ and n. Details of this calculation are omitted as it closely follows the equivalent calculation for a spherical void given by Budiansky *et al.* (1982). We find, for large $\dot V/(\dot\gamma V)$,

$$\frac{\dot V}{\dot\gamma V} = \mathrm{sgn}\left(\frac{\sigma_m}{\tau}\right) \left\{ \frac{1}{n} \left| \frac{\sigma_m}{\tau} \right| + \frac{(n-1)(n+g)}{n^2} \right\}^n, \quad (4.2)$$

where

$$g = \lim_{\epsilon \to 0} \left[\ln \epsilon - \frac{1}{\pi} \int_0^{\pi} \mathrm{d}\theta \int_{\epsilon}^{\infty} \{ z^{-2}(1 - 2z \sin 2\theta + z^2)^{\frac{1}{2}} - z^{-1} - z^{-2} \} \, \mathrm{d}z \right]$$
$$= 2 - \ln 4 = 0.6137. \quad (4.3)$$

Equation (4.2) is exact for $n = 1$; for $n \to \infty$ it becomes

$$\dot V/\dot\gamma V = \exp(g-1) \exp(\sigma_m/\tau) = 0.680 \exp(\sigma_m/\tau), \quad (4.4)$$

which is the counterpart to the result of Rice & Tracey (1969) for a spherical void. The high triaxiality predictions from (4.2) are compared with the more accurate numerical results from §2.3 in figure 12. The approximation gives good agreement for $\sigma_m/\tau > 4$, and even for σ_m/τ as small as unity it underestimates the dilatation rate by no more than 30 %.

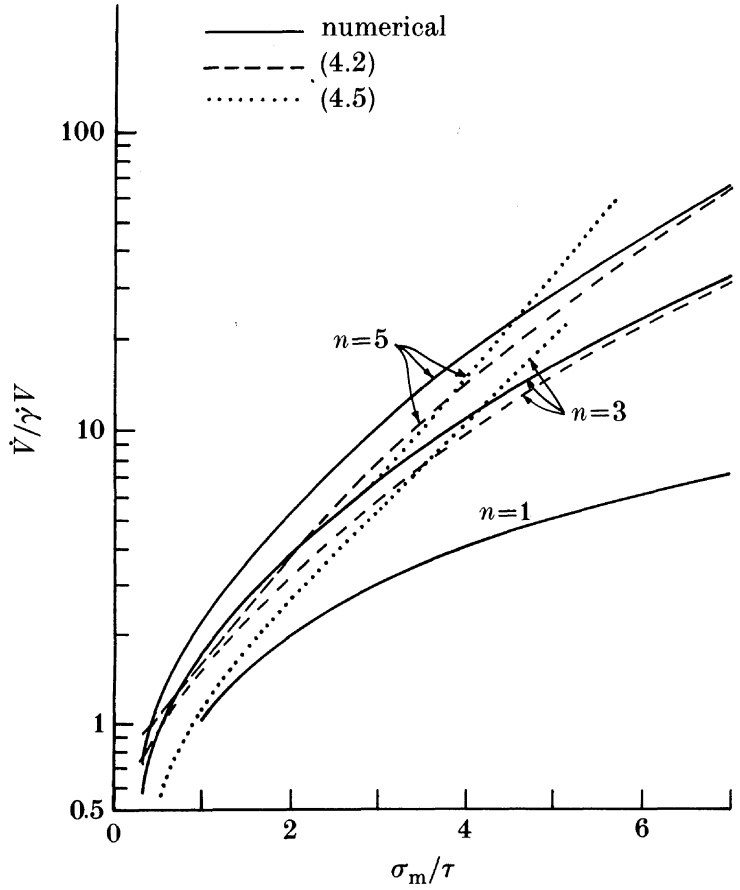

FIGURE 12. Normalized dilatation rate of a void of circular cross section as a function of stress triaxiality σ_m/τ. Comparison of the numerical results with the high triaxiality approximation (4.2) and the approximation (4.5) of McClintock *et al.* (1966).

Included in figure 12 is the dilatation rate from the formula

$$\dot{V}/\dot{\gamma}V = (n/(n-1))\sinh[((n-1)/n)\,\sigma_m/\tau], \tag{4.5}$$

from McClintock *et al.* (1966), who arrived at this approximate formula by converting a result for the axisymmetric deformation of a circular cylindrical void to the shear loading. This result is not accurate at very high triaxiality (except for the case $n = 1$, when it is exact) and is somewhat less accurate than (4.2) for σ_m/τ in the range from 1 to 4.

The high triaxiality approximation (4.2) is exact in the limit of pure hydrostatic loading. Multiplying (4.2) by $\eta\dot{\gamma} = (|\tau|\sqrt{3})^{n-1}\tau$ gives

$$\eta\dot{V}/V = (\sqrt{3})^{n-1}\{(1/n)|\sigma_m| + [(n-1)(n+g)/n^2]\,|\tau|\}^n \operatorname{sgn}(\sigma_m). \tag{4.6}$$

The nonlinear coupling between τ and σ_m in giving large dilatation rates in the

high triaxiality range can be seen very clearly from (4.6). As an illustration for $n = 5$, the dilatation rate of a cylindrical void under combined σ_m and τ with $\tau = \sigma_m/4$ is 40 times greater than the corresponding dilatation rate under the same hydrostatic stress σ_m with $\tau = 0$.

4.2. *Low triaxiality approximation*

When $|\sigma_m/\tau| < 1$, the dilatation rate of a circular cylindrical void is almost linear in σ_m/τ as can be seen in figure 6. Thus, an accurate low triaxiality approximation for the normalized dilatation rate is

$$\dot{V}/\dot{\gamma}V = \kappa(n)\,\sigma_m/\tau. \tag{4.7}$$

Values of $\kappa(n)$ have been calculated from the average slope of the relation between $\dot{V}/\dot{\gamma}V$ and σ_m/τ over the range between $\sigma_m/\tau = 0$ and $\frac{1}{3}$, and these are presented in table 1. Both the present result (4.7) and (4.5) of McClintock *et al.* are exact for $n = 1$, but (4.5) is significantly in error in the low triaxiality range for $n > 1$.

TABLE 1. LOW TRIAXIALITY APPROXIMATION FOR DILATATION RATE OF CIRCULAR CYLINDRICAL VOID

n	$\kappa(n)$	$f^*(n)$
1	1	1
3	1.742	1.600
5	2.209	1.898
7	2.529	2.090

The high and low triaxiality formulas cover essentially the entire range of triaxiality, albeit with errors which may be as large as 30 % for σ_m/τ in the vicinity of 2. A uniform approximation over the entire range of triaxiality could be developed but this is not pursued here.

5. CONSTITUTIVE POTENTIAL FOR A POWER-LAW VISCOUS SOLID CONTAINING A DILUTE CONCENTRATION OF CIRCULAR CYLINDRICAL VOIDS

The solution for the circular cylindrical void produced above can be used to derive the relation between overall strain rate and stress of a block of material containing a dilute, random array of aligned circular cylindrical voids. Plane strain deformation of the block is assumed with no straining parallel to the cylindrical axes of the voids. The theory below follows the approach of Duva & Hutchinson (1984) that was spelled out in some detail for spherical voids. The constitutive potential of the matrix material is defined by

$$\phi(\boldsymbol{\sigma}) = \int_0^{\boldsymbol{\sigma}} \epsilon_{ij}\,\mathrm{d}\sigma_{ij} = \frac{1}{3\eta}\frac{\sigma_e^{n+1}}{n+1}, \tag{5.1}$$

so that

$$\epsilon_{ij} = \partial\phi/\partial\sigma_{ij} = (1/(2\eta))\,\sigma_e^{n-1}s_{ij}. \tag{5.2}$$

Let $\bar{\boldsymbol{\sigma}}$ and $\bar{\boldsymbol{\varepsilon}}$ denote the macroscopic, or average, stress and strain rate of a representative block of the material of volume V containing a distribution of voids. The macroscopic constitutive potential $\boldsymbol{\Phi}(\bar{\boldsymbol{\sigma}})$ of the block provides the macroscopic strain rate according to

$$\bar{\epsilon}_{ij} = \partial\boldsymbol{\Phi}/\partial\bar{\sigma}_{ij}, \tag{5.3}$$

where $\boldsymbol{\Phi}$ is related to the distribution of the local potential by

$$V\boldsymbol{\Phi}(\bar{\boldsymbol{\sigma}}) = \int_{V_m} \phi(\boldsymbol{\sigma})\,\mathrm{d}V, \tag{5.4}$$

with V_m denoting the region occupied by the matrix material.

For a dilute concentration of voids with volume fraction (or area fraction) ρ, the macroscopic potential can be written as

$$\boldsymbol{\Phi}(\bar{\boldsymbol{\sigma}}) = \phi(\bar{\boldsymbol{\sigma}}) + \rho\boldsymbol{\Phi}_v(\bar{\boldsymbol{\sigma}}), \tag{5.5}$$

where $\boldsymbol{\Phi}_v(\bar{\boldsymbol{\sigma}})$ is an appropriately defined change in potential due to the introduction of an isolated void of unit volume (or unit area) into an infinite block of matrix material that is subject to remote stress $\boldsymbol{\sigma}^\infty = \bar{\boldsymbol{\sigma}}$.

To define $\boldsymbol{\Phi}_v$, first consider the problem of an isolated void centered in a spherical (or cylindrical) matrix of finite outer radius a_0, where uniform tractions $T_i = \sigma_{ij}^\infty n_j$ are applied to the outer surface of the matrix. Define the *change* in the potential due to the introduction of the void as

$$V_v\,\boldsymbol{\Phi}_v(\boldsymbol{\sigma}^\infty) = \int_{V_m} [\phi(\boldsymbol{\sigma}) - \phi(\boldsymbol{\sigma}^\infty)]\,\mathrm{d}V - V_v\,\phi(\boldsymbol{\sigma}^\infty), \tag{5.6}$$

where V_v is the volume of the void and V_m denotes the region occupied by the matrix.

With
$$\epsilon_{ij}^\infty = (\partial\phi/\partial\sigma_{ij})_{\boldsymbol{\sigma}=\boldsymbol{\sigma}^\infty} \tag{5.7}$$

and noting that

$$\int_{V_m} (\sigma_{ij} - \sigma_{ij}^\infty)\,\epsilon_{ij}^\infty\,\mathrm{d}V = V_v\,\sigma_{ij}^\infty\,\epsilon_{ij}^\infty, \tag{5.8}$$

one can rewrite (5.6) as

$$V_v\,\boldsymbol{\Phi}_v(\boldsymbol{\sigma}^\infty) = \int_{V_m} [\phi(\boldsymbol{\sigma}) - \phi(\boldsymbol{\sigma}^\infty) - (\sigma_{ij} - \sigma_{ij}^\infty)\,\epsilon_{ij}^\infty]\,\mathrm{d}V + V_v\,w(\boldsymbol{\varepsilon}^\infty), \tag{5.9}$$

where $w(\boldsymbol{\varepsilon}) + \phi(\boldsymbol{\sigma}) = \sigma_{ij}\,\epsilon_{ij}$ has been used. Now let the outer radius a_0 become unbounded to obtain $\boldsymbol{\Phi}_v$ for the isolated void. The advantage of (5.9) over (5.6) is that the integrand of the volume integral in (5.9) decays sufficiently rapidly at large distances from the void such that $\boldsymbol{\Phi}_v$ can be evaluated either as the limit of the finite problem as the outer radius a_0 becomes unbounded *or* directly from the infinite problem where the remote stress is $\boldsymbol{\sigma}^\infty$. As it stands, (5.6) cannot be used to evaluate $\boldsymbol{\Phi}_v$ directly from the infinite problem.† We also note the

† This corrects the statement made by Duva & Hutchinson (1984) with respect to the definition (5.6).

connection between Φ_v and the minimum of the functional P defined by (2.9),

$$P_{\min} + V_v \Phi_v = V_v w(\varepsilon^\infty), \tag{5.10}$$

which is most readily established by adding together the right and left hand sides of (5.9) and (2.9).

For a circular cylindrical void in an infinite matrix subject to plane strain deformations, Φ_v is a homogeneous function of degree $n+1$ in the remote stress and is an isotropic function of the in-plane components of $\boldsymbol{\sigma}^\infty$. Without loss of generality, Φ_v can be written as

$$\Phi_v(\boldsymbol{\sigma}^\infty) = (1/(3\eta))\,(\sigma_e^\infty)^{n+1} f(X, n), \tag{5.11}$$

where $\sigma_e^\infty = (3 s_{ij}^\infty s_{ij}^\infty/2)^{\frac{1}{2}}$, and

$$X = \sigma_m^\infty/\sigma_e^\infty. \tag{5.12}$$

Moreover, f is an even function of X.

To obtain $f(X, n)$, we use the fact that the dilatation rate of the void is given by

$$\dot{V}_v/V_v = \partial\Phi_v/\partial\sigma_m^\infty = (1/(3\eta))\,\sigma_e^n\,\partial f/\partial X. \tag{5.13}$$

For the remote stress state (1.3), $\sigma_e^\infty = |\tau|\sqrt{3}$ and $\eta\dot{\gamma} = (|\tau|\sqrt{3})^{n-1}\tau$ so that

$$\dot{V}_v/\dot{\gamma} V_v = (\operatorname{sgn}(\tau)/\sqrt{3})\,\partial f/\partial X. \tag{5.14}$$

In the *high triaxiality range*, an approximation to $\partial f/\partial X$ is obtained immediately by comparing (5.14) with (4.2). To within an unknown constant of integration f is therefore given by

$$f(X, n) = (n/(n+1))\,[|X|\sqrt{3}/n + (n-1)\,(n+g)/n^2]^{n+1}. \tag{5.15}$$

For large X the constant of integration is asymptotically negligible, and no attempt has been made to determine it. Similarly, in the *low triaxiality range* an approximation to f is obtained by comparing (5.14) with (4.7), giving

$$f(X, n) = f^*(n) + \tfrac{3}{2}\kappa(n)\,X^2, \tag{5.16}$$

where the constant of integration f^* must now be retained. Values of $f^*(n)$ were found from the computed values of $P_{\min}$ when $X = 0$ via (5.10), by using the numerical technique of §2. These values are included in table 1. For $n = 1$, (5.16) becomes

$$f = 1 + \tfrac{3}{2}X^2, \tag{5.17}$$

and this result is exact for all X.

The high and low triaxiality approximations to f in (5.15) and (5.16) are compared with the more accurate full numerical calculations of f in figure 13. The full numerical results were obtained from the results of §2 by using (5.10). The approximations are quite good in their respective ranges.

With the void potential Φ_v in hand, one can use (5.3) and (5.5) to obtain the

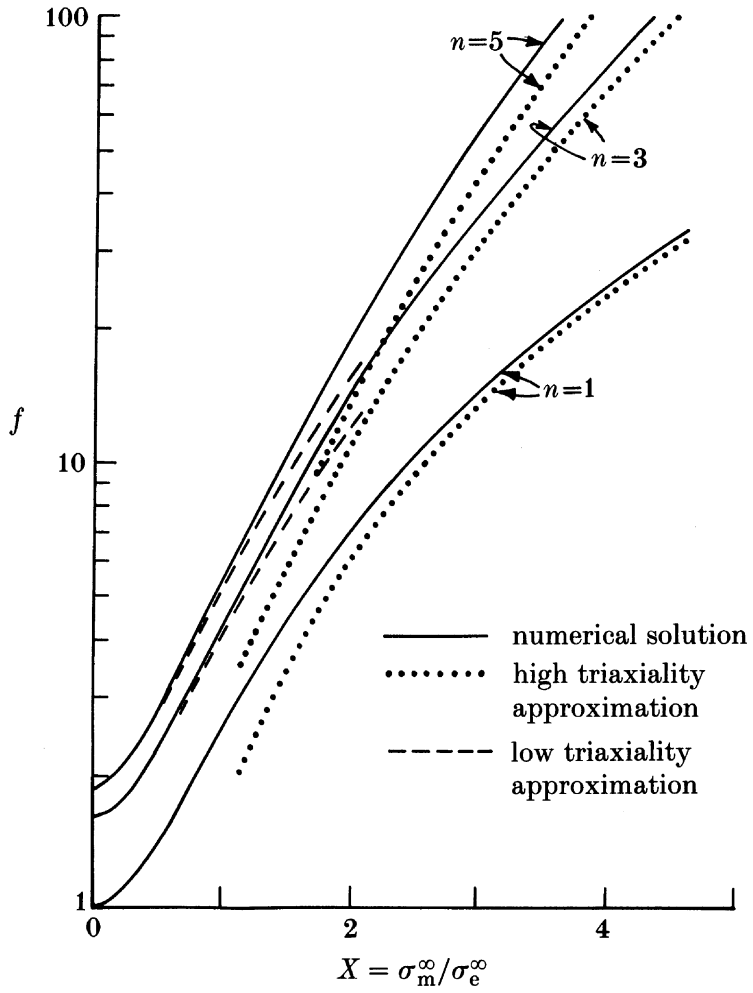

FIGURE 13. Numerical results for $f(X, n)$ defining the void potential in (5.11), and comparisons with (5.15) derived from the high triaxiality approximation and (5.16) derived from the low triaxiality approximation.

overall strain rate of the block containing a dilute distribution of circular cylindrical voids and undergoing plane strain deformations. The result is

$$\bar{\epsilon}_{\alpha\beta} = \frac{1}{2\eta}(\bar{\sigma}_e)^{n-1}\bar{s}_{\alpha\beta} + \frac{\rho}{3\eta}(\bar{\sigma}_e)^n\left[\frac{3}{2}\frac{\bar{s}_{\alpha\beta}}{\bar{\sigma}_e}\left\{(n+1)f - X\frac{\partial f}{\partial X}\right\} + \frac{1}{3}\frac{\partial f}{\partial X}\delta_{\alpha\beta}\right], \qquad (5.18)$$

where the notation for the barred quantities is consistent with earlier notation and where α and β range over the indices 1 and 2. The approximations for f in (5.15) and (5.16) may be inserted for the appropriate range of triaxiality.

6. Concluding discussion and a summary of results for voids and cracks subject to shear

The present study has brought out the strong coupling between mean stress σ_m and shear stress τ in the determination of the dilatation rate of the void. In addition, nonlinearity has a significant effect on the asymptotic orientation of an

isolated void under combined stress. At large values of triaxiality (i.e. large σ_m/τ) the void grows most rapidly in the direction transverse to the direction of maximum principal strain rate. The present results for nonlinear materials were limited to cylindrical voids. Nevertheless, because there appears to be a fairly close parallel between the behaviour of the 2D void and the 3D void, we expect many of the qualitative features identified for the 2D problem to pertain to 3D voids. In particular, it appears from the results presented here and elsewhere (Budiansky & Hutchinson 1980) that the dilatation rate of a void (2D or 3D) which has attained its asymptotic, steady-state shape is the same, or approximately the same, for the nonlinear material, as the dilatation rate of a circular (in 2D) or spherical (in 3D) void. The generality of this result remains to be seen.

We conclude the paper by presenting table 2, which collects together results for the dilatation rates of isolated voids and cracks under combined remote mean stress σ_m and shear stress τ. The first entry gives the present results for the high and low triaxiality approximations for the circular cylindrical void undergoing plane strain deformations. The second entry gives the corresponding results for a spherical void subject to the same remote stress conditions. These are the results of Budiansky *et al.* (1982) that were derived by assuming axisymmetric stressing for arbitrary combinations of remote invariants σ_m and σ_e. Their results have been translated to the shear problem by identifying σ_e with $\sqrt{3}|\tau|$. The last entry in table 2 is that for a crack of length $2a$ in the power-law viscous solid undergoing plane strain deformation and subject to a remote mean stress σ_m and shear stress τ parallel to the crack. The dilatation rate is obtained as follows from an approximate solution for the J-integral for this crack problem given by M. Y. He (personal communication 1985). He's formula is

$$J = (\tfrac{1}{4}\pi\sqrt{n})\,[1+(\sigma_m/\tau)^2]\,\tau\dot{\gamma}a. \tag{6.1}$$

Now, J is directly related to the crack potential Φ_c by $J = (\frac{1}{2})\,\partial\Phi_c/\partial a$ where, in analogy to the void problem, Φ_c is the change in potential (per unit thickness) from the introduction of the crack. Thus,

$$\Phi_c = (\tfrac{1}{4}\pi\sqrt{n})\,[1+(\sigma_m/\tau)^2]\,\tau\dot{\gamma}a^2, \tag{6.2}$$

and the rate of change of the cross-sectional area of the crack is therefore

$$\dot{A} = \partial\Phi_c/\partial\sigma_m = (\tfrac{1}{2}\pi\sqrt{n})\,(\sigma_m/\tau)\,\dot{\gamma}a^2. \tag{6.3}$$

The normalized rate $\dot{A}/(\dot{\gamma}\pi a^2)$ is listed in table 2. Based on numerical comparisons, He suggests that (6.1) is reasonably accurate as long as $|\sigma_m/\tau|$ does not exceed 3 or 4, and we suppose the same limitation applies to (6.3). The formulas (6.1)–(6.3) are exact for $n = 1$.

Lastly, we have noted in table 2 that the normalized dilatation rate for the circular cylindrical void in the low triaxiality range is well approximated (to within 5 % for all n computed) by $\sqrt{n}\sigma_m/\tau$. This is exactly twice the normalized rate $\dot{A}/(\dot{\gamma}\pi a^2)$ for the crack.

TABLE 2

Cylindrical void

high triaxiality $|\sigma_m/\tau| > 1$

$$\frac{\dot{V}}{\dot{\gamma} V} = \left\{\frac{1}{n}\left|\frac{\sigma_m}{\tau}\right| + \frac{(n-1)(n+0.6137)}{n^2}\right\}^n \cdot \operatorname{sgn}\left(\frac{\sigma_m}{\tau}\right)$$

low triaxiality $|\sigma_m/\tau| \leqslant 1$

$$\frac{\dot{V}}{\dot{\gamma} V} = \kappa(n)\frac{\sigma_m}{\tau} \approx \sqrt{n}\frac{\sigma_m}{\tau}$$

Both formulae are exact for $n = 1$.

n	$\kappa(n)$
1	1
3	1.742
5	2.209
7	2.529

Spherical void

high triaxiality $|\sigma_m/\tau| > 2$

$$\frac{\dot{V}}{\dot{\gamma} V} = \frac{\sqrt{3}}{2}\left\{\frac{\sqrt{3}}{2n}\left|\frac{\sigma_m}{\tau}\right| + \frac{(n-1)(n+0.4319)}{n^2}\right\}^n \cdot \operatorname{sgn}\left(\frac{\sigma_m}{\tau}\right)$$

low triaxiality $|\sigma_m/\tau| \leqslant 2$

$$\frac{\dot{V}}{\dot{\gamma} V} = \frac{\kappa(n)}{3}\frac{\sigma_m}{\tau}$$

Both formulae are exact for $n = 1$.

n	$\kappa(n)$
1	2.25
1.5	2.42
2	2.55
3	2.71
5	2.88
10	3.06
∞	3.30

Plane strain crack

low to moderate triaxiality $|\sigma_m/\tau| \leqslant 3$

$$\frac{\dot{A}}{\dot{\gamma}\pi a^2} = \frac{\sqrt{n}}{2}\frac{\sigma_m}{\tau}$$

Exact for $n = 1$.

The work of N.A.F. was supported in part by a Lindemann Trust Fellowship, the National Science Foundation under Grant MEA-82-13925 and the Division of Applied Sciences. The work of J.W.H. was supported in part by the National Science Foundation under Grants DMR-83-16979 and MSM-84-16392, and the Division of Applied Sciences, Harvard University.

Appendix: some details of the numerical solution

Evaluation of the additional velocities and strain rates requires evaluation of the following partial derivatives of the stream function: $\chi_{,1}$, $\chi_{,2}$, $\chi_{,11}$, $\chi_{,12}$, and $\chi_{,22}$. The stream function in (2.13) is represented as a function of the polar variables (μ, ϕ) in the mapped plane. By a change of variables

$$\chi_{,1} = \chi_{,\mu}\mu_{,1} + \chi_{,\phi}\phi_{,1}, \tag{A 1}$$

$$\chi_{,11} = (\chi_{,\mu\mu}\mu_{,1} + \chi_{,\mu\phi}\phi_{,1})\mu_{,1} + \chi_{,\mu}\mu_{,11} + (\chi_{,\mu\phi}\mu_{,1} + \chi_{,\phi\phi}\phi_{,1})\phi_{,1} + \chi_{,\phi}\phi_{,11}, \tag{A 2}$$

with similar expressions for the other partial derivatives. The mapping function $z = \omega(\zeta)$ can be used to obtain the values of $\mu_{,1}$, $\mu_{,11}$, etc. These relations are similar to those of Budiansky & Hutchinson (1980), i.e.

$$\mu_{,1} - \mathrm{i}\mu_{,2} = \mu/\Omega, \quad \phi_{,2} + \mathrm{i}\phi_{,1} = 1/\Omega,$$

$$\mu_{,11} + \mathrm{i}\mu_{,12} = \mu_{,1}\Omega/|\Omega|^2 + \mu\Omega'/(|\Omega|^2\omega') - (2\mu\Omega/|\Omega|^4)\,\mathrm{Re}\{\bar{\Omega}\Omega'/\omega'\}$$

$$\mu_{,12} + \mathrm{i}\mu_{,22} = \mu_{,2}\Omega/|\Omega|^2 + \mathrm{i}\mu\Omega'/(|\Omega|^2\omega') - (2\mu\Omega/|\Omega|^4)\,\mathrm{Re}\{\mathrm{i}\bar{\Omega}\Omega'/\omega'\}$$

$$\phi_{,22} - \mathrm{i}\phi_{,12} = \mathrm{i}\Omega'/(|\Omega|^2\omega') - (2\Omega/|\Omega|^4)\,\mathrm{Re}\{\mathrm{i}\bar{\Omega}\Omega'/\omega'\}$$

$$\phi_{,12} - \mathrm{i}\phi_{,11} = \Omega'/(|\Omega|^2\omega') - (2\Omega/|\Omega|^4)\,\mathrm{Re}\{\bar{\Omega}\Omega'/\omega'\}$$

where $\Omega = \zeta\omega'$, $(\,)' = \mathrm{d}(\,)/\mathrm{d}\zeta$ and $\bar{(\,)}$ denotes the complex conjugate. Thus, the additional velocities and strain rates at the point z associated with ζ are readily computed when the amplitude factors $\{A_p\}$ are assigned numerical values.

The integrals in (2.9), (2.17) and (2.18) were obtained numerically using a ten-point Gaussian quadrature formula. The double integrals were evaluated by subdividing the range of each of μ onto ϕ into two equal intervals and applying the Gauss formula in each subinterval. In all, 20×20 points were used in the evaluation. Various checks were made to ensure that the integrals were evaluated accurately with this procedure.

References

Bilby, B. A., Eshelby, J. D. & Kundu, A. K. 1975 *Techtonophysics* **28**, 265.

Bilby, B. A. & Kolbuszewski, M. L. 1977 *Proc. R. Soc. Lond.* A **355**, 335.

Budiansky, B. & Hutchinson, J. W. 1980 In *Proc. of XVth int. congress of theoretical and applied mechanics, Toronto, Canada, 17–23 August* 1980 (ed. F. P. J. Rimrott & B. Tabarrok), p. 243. North-Holland Publishing Co.

Budiansky, B., Hutchinson, J. W. & Slutsky, S. 1982 In *Mechanics of solids* (ed. H. G. Hopkins & M. J. Sewell) p. 13. Oxford: Pergamon Press.

Duva, J. M. & Hutchinson, J. W. 1984 *Mech. Mater.* **3**, 41.

Eshelby, J. D. 1957 *Proc. R. Soc. Lond.* A **241**, 376.

Goddard, J. D. & Miller, C. 1967 *J. Fluid Mech.* **28**, 657.

Hill, R. 1956 *J. Mech. Phys. Solids* **5**, 66.

Howard, I. C. & Brierley, P. 1976 *Int. J. Engng Sci.* **14**, 1151.

McClintock, F. A., Kaplan, S. M. & Berg, C. A. 1966 *Int. J. Fracture Mech.* **2**, 614.

Rice, J. R. & Tracey, D. M. 1969 *J. Mech. Phys. Solids* **17**, 201.